



Simulation of Strong Ground Motions at Onagawa, Japan, during the 2011 off Miyagi, Intra-slab Earthquake by Empirical Green's Function Method

A. Oana⁽¹⁾, K. Dan⁽²⁾, J. Miyakoshi⁽³⁾, K. Ishikawa⁽⁴⁾, T. Fukushima⁽⁵⁾

⁽¹⁾ Institute of Technology, Shimizu Corporation, a.oana@shimz.co.jp

⁽²⁾ Research fellow, Ohsaki Research Institute, Inc., kazuo.dan@ohsaki.co.jp

⁽³⁾ Director of the Research Dept., Ohsaki Research Institute, Inc., Miyakoshi@ohsaki.co.jp

⁽⁴⁾ Deputy director, Tohoku Electric Power Company, ishikawa.kazuya.jp@tohoku-epco.co.jp

⁽⁵⁾ Deputy director, Tohoku Electric Power Company, fukushi.tomoji.wy@tohoku-epco.co.jp

Abstract

We simulated the strong motions at Onagawa, Japan, during the 2011 off Miyagi intra-slab earthquake (Mw7.1) by the empirical Green's function method. We used some different elemental earthquakes in order to investigate the applicability of this method for the intra-slab earthquakes. At first, we established the asperity model based on the previous study. Then, the elemental earthquakes were selected under some criteria. Finally, we carried out the strong motion simulations for three models: using only one elemental earthquake (Model 1), using three elemental earthquakes which were arranged according to the relationship between their source locations and the subfaults of the target large fault (Model 2), and using three elemental earthquakes which were arranged randomly (Model 3). For the model 1, the variation of the simulated strong motions to the observed strong motion was large. On the other hand, for the models 2 and 3, the variation of the simulated strong motions to the observed strong motion was smaller than that of the model 1 because the characteristics of each elemental earthquake were averaged. This conclusion agrees with that in Dan et al. (1990) for a crustal earthquake.

Keywords: Empirical Green's function method, 2011 off Miyagi earthquake, Intra-slab earthquake



1. Introduction

The empirical Green's function method (Hartzell, 1978) has often been used for the strong motion prediction. In this method, the elemental earthquakes are used as the empirical Green's functions, and they are scaled so that their fault parameters are the same as those of the subfaults of the target large fault. If several strong motion records have been observed at the site, all of them should be used as elemental earthquakes because the specific characteristics of the amplification and the propagation can be taken into account. Many studies have applied this method to the strong motion simulations for large earthquakes. For example, Dan et al. (1990) examined the variation of the strong motions synthesized by using several small-event records as Green's functions for a crustal earthquake. They arranged the small-event records randomly for each subfault of the main-shock, and showed that the variation of the simulated strong motions became small. Miyakoshi et al. (2004) estimated the strong motions using some elemental earthquakes for a scenario interplate earthquake along the Nankai trough, Japan.

In this paper, we simulated the strong motions at Onagawa during the 2011 off Miyagi intra-slab earthquake (Mw7.1) by the empirical Green's function method using some different elemental earthquakes in order to investigate the applicability of this method to the intra-slab earthquake.

2. Fault Model

We established an asperity model for the 2011 off Miyagi earthquake after the seismic moment M_0 , the short-period spectral level A , and the ratio of the asperity areas to the seismic fault area S_a/S were given. The seismic moment M_0 was 4.74×10^{19} Nm (NIED, 2011). The short-period spectral level A was 1.16×10^{20} Nm/s² which was evaluated from the stress drops of the strong motion generation areas obtained by Harada and Kamae (2011) (HKmodel). The relationship between the seismic moment M_0 and the short-period spectral level A is shown in Figure 1. The short-period spectral level A is about 6 times as large as the empirical relationship between the seismic moment and the short-period spectral level proposed by Dan et al. (2001), about 1.5 times as large as the empirical relationship by Sasatani et al. (2006). It is almost the same as the empirical relationship by Arai et al. (2015). The ratio of the asperity areas to the entire seismic fault area S_a/S was obtained to be 0.4 based on our pre-studies. The strike and the dip of the fault model were taken as 20° and 37° , respectively, in reference to some previous studies. Two asperities were arranged apart in the asperity model based on the HKmodel. The asperity model is shown in Figure 2. The fault parameters are shown in Table 1.

3. Elemental Earthquakes

3.1 Selection of the elemental earthquakes

The elemental earthquakes for the strong motion simulations by the empirical Green's function method were selected based on the following five criteria:

- 1) The source locates close to the main-shock source.
- 2) The ratio of signal to noise of the Fourier amplitude spectrum of the observed strong motion at Onagawa in the period range of 10 seconds or less is large enough.
- 3) The seismic moment is given by F-net.
- 4) The moment magnitude M_w is larger than 4.5.
- 5) The focal mechanism is similar to the main-shock.

The source parameters of the main-shock and selected elemental earthquakes are shown in Table 2. The map including the locations of the main-shock, selected elemental earthquakes, fault plane of the main-shock, and Onagawa site are shown in Figure 3.

3.2 Estimation of the Source Parameters of the Main-shock and the Elemental Earthquakes

The source spectrum of the main-shock was assumed as the following stochastic model based on Boore (1983):



$$S(f) = AMP(f) \cdot \frac{4\pi\rho\beta^3}{R_{\theta\phi}F_S P} \cdot \exp\left(\frac{\pi f R}{Q(f)\beta}\right) R \cdot \sqrt{\frac{\rho_S \beta_S}{\rho\beta}}, \quad (1)$$

where f is the frequency, $S(f)$ is the acceleration source spectrum, $AMP(f)$ is the acceleration Fourier amplitude spectrum of the observed strong motion records, R is the hypocentral distance, $R_{\theta\phi}$ is the radiation pattern, usually averaged over a suitable range of azimuths and take-off angles (Boore and Boatwright, 1984), F_S is the effect of the free surface (taken as 1 because we use the underground records), P represents the partition of total shear-wave energy into horizontal components ($=1/\sqrt{2}$), $Q(f)$ is the function which represents attenuation of the path (assuming $114f^{0.92}$: Satoh and Tatsumi, 2002), ρ_S and β_S are the density and shear-wave velocity of the observation point (Onagawa), and ρ and β are the density and shear-wave velocity at the source. The third and last terms of the RHS mean the path characteristic and the amplification characteristic, respectively.

The theoretical source spectrum of the main-shock was estimated by the following ω -square model (Brune, 1970):

$$S(f) = \frac{(2\pi f)^2 M_0}{1 + (f/f_c)^2}, \quad (2)$$

where f_c is the corner frequency. The corner frequency f_c was derived from the seismic moment M_0 and the short-period spectral level A by

$$f_c = \frac{1}{2\pi} \sqrt{\frac{A}{M_0}}. \quad (3)$$

The source spectra of the main-shock and the elemental earthquakes were assumed to be represented by equation (1). The seismic moments M_0 were taken from F-net (NIED, 2011), and the corner frequencies f_c were estimated based on the ratio of the source spectrum of the main-shock to that of the elemental earthquake. In concrete, the corner frequencies of the elemental earthquakes were evaluated so that the theoretical source spectral ratio of the main-shock to each elemental earthquake becomes almost the same as the source spectral ratio based on the observed strong motions in 1-5 Hz. The ratios of the source spectrum of the main-shock to that of the elemental earthquake are shown in Figure 4. The estimated source parameters of the elemental earthquakes are shown in Table 3.

4. Strong Motion Simulations by the Empirical Green's Function Method

We carried out the strong motion simulations of the off Miyagi earthquake by three models: using only one elemental earthquake (Model 1), using three elemental earthquakes which were arranged according to the relationship between their source locations and the subfaults (Model 2), and using three elemental earthquakes which were arranged randomly (Model 3). The arrangements of the elemental earthquake(s) for the subfaults in the fault model are shown in Figure 5. The model 3 in Figure 5 shows two representative cases which were selected from 100 cases. The peak ground accelerations and the pseudo-velocity response spectra of these two cases corresponded well to those of the observed strong motions.

The rupture velocity was assumed to be 2.88 km/s, which is 0.72β (Geller, 1976). The underground observed strong motions of the elemental earthquakes, rotated from the sensor N-S direction to the plant N-S direction, were used as the elemental strong motions. We calculated 21 waves in which we changed the radiation location of the seismic waves in the subfault randomly in each model in order to avoid causing artificial waves. Then, we selected one wave whose pseudo-velocity response spectrum was almost the same as the averaged one.

The simulated strong motions of the model 1 are shown in Figure 6. The period characteristic and the difference of the two horizontal components observed in the records of the elemental earthquakes have also appeared in the simulated strong motions. As shown in Figure 6, the variation of the simulated strong motions to the observed strong motion is large. The simulated strong motions of the model 2 are shown in Figure 7. As shown in Figure 7, the simulated strong motions of the model 2 correspond with the observed records better than those of the model 1, while the pseudo-velocity response spectra of the simulated strong motions are larger than those of the



observed records in the period range larger than 1 second. The simulated strong motions of the model 3 are shown in Figure 8. The peak ground accelerations and the pseudo-velocity response spectra in the short-period range correspond well to those of the observed records because the characteristics of each elemental earthquake are averaged. The variation of the simulated strong motions to the observed strong motions is smaller than that of the model 1. However, the envelopes of the simulated strong motions are sharp. As a result, the reproducibility of the observed record of the model 3 is the best in the three models.

5. Conclusion

We simulated the strong ground motions at Onagawa, Japan for the 2011 off Miyagi intra-slab earthquake by the empirical Green's function method with using one or some elemental earthquakes.

The model 1 was established by using only one elemental earthquake. The variation of the simulated strong motions to the observed strong motion was large.

The model 2 was established by using three elemental earthquakes which were arranged according to the relationship between their source locations and subfaults of the target large fault. The simulated strong motions of the model 2 corresponded to the observed records better than those of the model 1. However, the pseudo-velocity response spectra were overestimated in the period range larger than 1 second.

The model 3 was established by using three elemental earthquakes which were arranged randomly. The simulated strong motions of the model 3 also showed better agreement with the observed strong motion records than those of the model 1. The variation of the simulated strong motions to the observed strong motion was smaller than that of the model 1. This conclusion agrees with that in Dan et al. (1990). The improvements of the sharp envelopes of the simulated strong motions are a future issue.

Finally, the results of this study showed that the empirical Green's function method of using some different elemental earthquakes is applicable for the intra-slab earthquake.

6. References

- [1] Hartzell SH (1978): Earthquake Aftershocks as Green's Functions. *Geophysical Research Letters*, Vol.5, pp.1-4.
- [2] Dan K, Watanabe T, Tanaka T, Sato R (1990): Stability of Earthquake Ground Motion Synthesized by Using Different Small-event Records as Empirical Green's Functions. *Bulletin of the Seismological Society of America*, Vol.80, No.6, pp.1433-1455.
- [3] Miyakoshi J, Nakata T, Fukuwa N, Shibata A, Shirase Y, Saito K (2004): Strong Motion Prediction for Retrofit of Buildings in the Sannomaru District of Nagoya City. Summaries of technical papers of Annual Meeting, Japan Association for Earthquake Engineering, pp.394-395.
- [4] Harada S, Kamae K (2011): Source Modeling of the off Miyagi Intraslab Earthquake of April 7, 2011. http://www.rri.kyoto-u.ac.jp/jishin/eq/tohoku2/20110407miyagioki_slab.pdf.
- [5] Dan K, Watanabe M, Sato T, Ishii T (2001): Short-period Source Spectra Inferred from Variable-slip Rupture Models and Modeling of Earthquake Faults for Strong Motion Prediction. *Journal of Structural and Construction Engineering (Transactions of the Architectural Institute of Japan)*, No.545, pp.51-62.
- [6] Sasatani T, Morikawa N, Maeda N (2006): Source Characteristics of Intraslab Earthquakes. *Geophysical Bulletin of Hokkaido University*, No.69, pp.123-134.
- [7] Arai K, Dan K, Ishii T, Hanamura M, Fujiwara H, Morikawa N (2015): Procedure of Evaluating Fault Parameters of Intra-slab Earthquakes for Strong Motion Prediction. *Journal of Structural and Construction Engineering (Transactions of the Architectural Institute of Japan)*, Vol.80, No.716, pp.1537-1547.
- [8] Boore DM (1983): Stochastic simulation of high-frequency ground motions based on seismological models of the radiated spectra. *Bulletin of the Seismological Society of America*, Vol.73, No.6, pp.1865-1894.
- [9] Boore DM, Boatwright J (1984): Average Body-wave Radiation Coefficients. *Bulletin of the Seismological Society of America*, Vol.74, No.5, pp.1615-1621.



- [10] National Research Institute for Earth Science and Disaster Resilience (2011, 2013): F-net(Broadband Seismograph Network), <http://www.fnet.bosai.go.jp/top.php?LANG=ja>.
- [11] Japan Meteorological Agency (2011, 2013): <http://www.jma.go.jp/jma/indexe.html>.
- [12] Satoh T, Tatsumi Y (2002): Source, Path, and Site Effects for Crustal and Subduction Earthquakes Inferred from Strong Motion Records in Japan. *Journal of Structural and Construction Engineering (Transactions of the Architectural Institute of Japan)*, No.556, pp.15-24.
- [13] Brune JN (1970): Tectonic Stress and the Spectra of Seismic Shear Waves from Earthquakes, *Journal of Geophysical Research*, Vol.75, No.26, pp.4997-5002.
- [14] Geller R (1976): Scaling Relations for Earthquake Source Parameters and Magnitudes. *Bulletin of the Seismological Society of America*, Vol.66, No.5, pp.1501-1523.

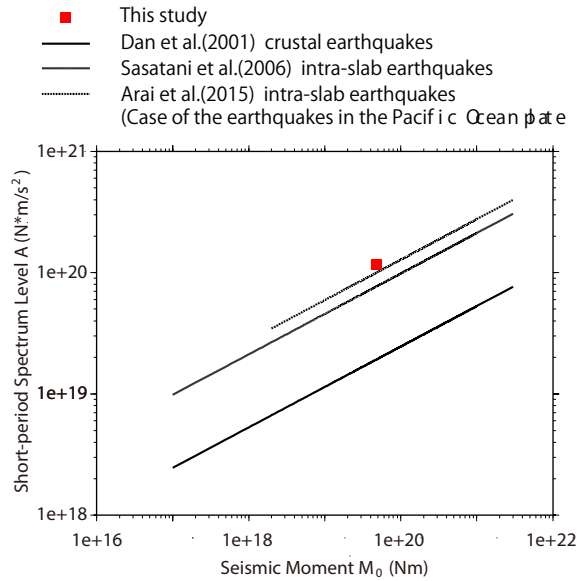


Figure 1 – Relationship between the seismic moment M_0 and the short-period spectral level A

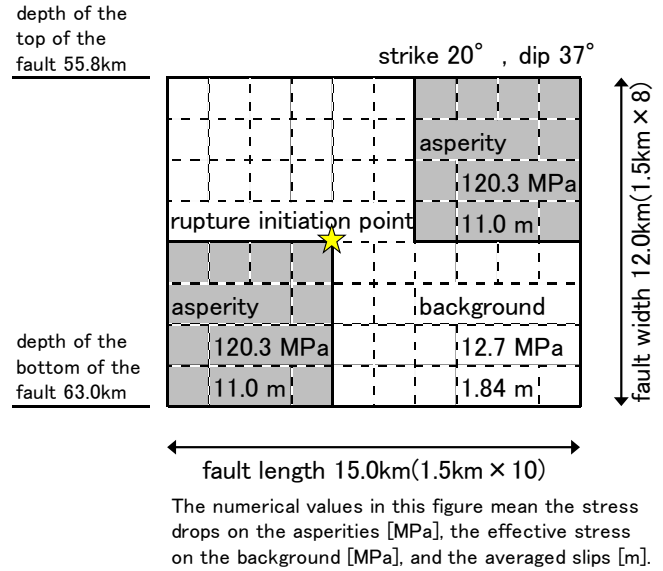


Figure 2 – Asperity model of the 2011 off Miyagi intra-slab earthquake

Table 1 – Fault parameters of the asperity model

Parameters		Basis
Seismic fault area S (km ²)	179.3	$S=(7/16)M_0 4\pi^2 \beta^2 / A (S/S_a)^{0.5}$
Seismic moment M_0 (Nm)	4.74E+19	NIED(2011)
Short-period spectral level A (Nm/s ²)	1.16E+20	Based on Harada and Kamae(2011).
Averaged stress drop $\Delta\sigma$ (MPa)	48.1	$\Delta\sigma=(7\pi^{1.5}/16)(M_0/S^{1.5})$
Averaged slip D (m)	5.51	$D=M_0/(\mu S)$
Combined asperity area S_a (km ²)	72	$S_a=(S_a/S)S$
Ratio of the asperity areas to the entire seismic fault area S_a/S	0.4	According to pre-study.
Stress drop on the asperities $\Delta\sigma_a$ (MPa)	120.3	$\Delta\sigma_a=\Delta\sigma/(S_a/S)$
Averaged slip on the asperities D_a (m)	11.0	$D_a=2D$
Effective stress on the background σ_b (MPa)	12.7	$\sigma_b=(D_b/W_b)(\pi^{0.5}/D_a)r \cdot \sum(r_i/r)^3 \Delta\sigma_a$
Averaged slip on the background D_b (m)	1.84	$D_b=M_{0b}/(\mu S_b)$

Table 2 – Source parameters of the main-shock and selected elemental earthquakes

	Time	Lat. *1	Lon. *1	M_0 (Nm) *1	Depth(km) *2	Mw
EQ04	2011/4/7 23:32	38.2028	141.9237	4.74E+19	66	7.1
EQ08	2011/4/9 18:42	38.2467	141.8160	1.21E+17	58	5.4
EQ26	2011/7/13 0:37	38.3312	142.0072	2.64E+16	47	4.9
EQ53	2013/8/4 12:29	38.1627	141.8025	6.86E+17	58	5.9

*1) NIED(2011, 2013) *2) JMA(2011, 2013)

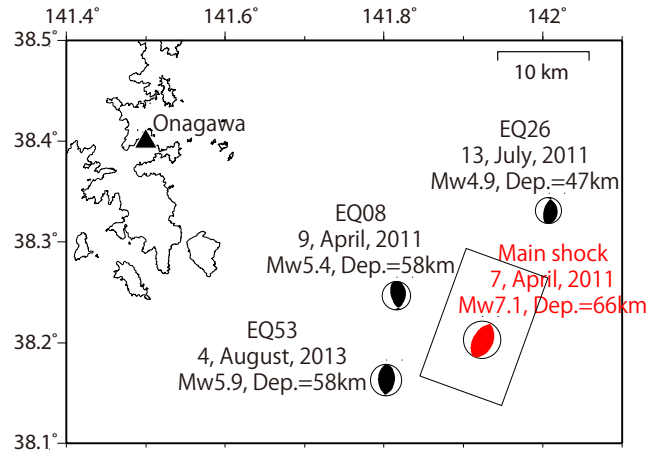


Figure 3 – Locations of the main-shock, selected elemental earthquakes, fault plane of the main-shock, and Onagawa site

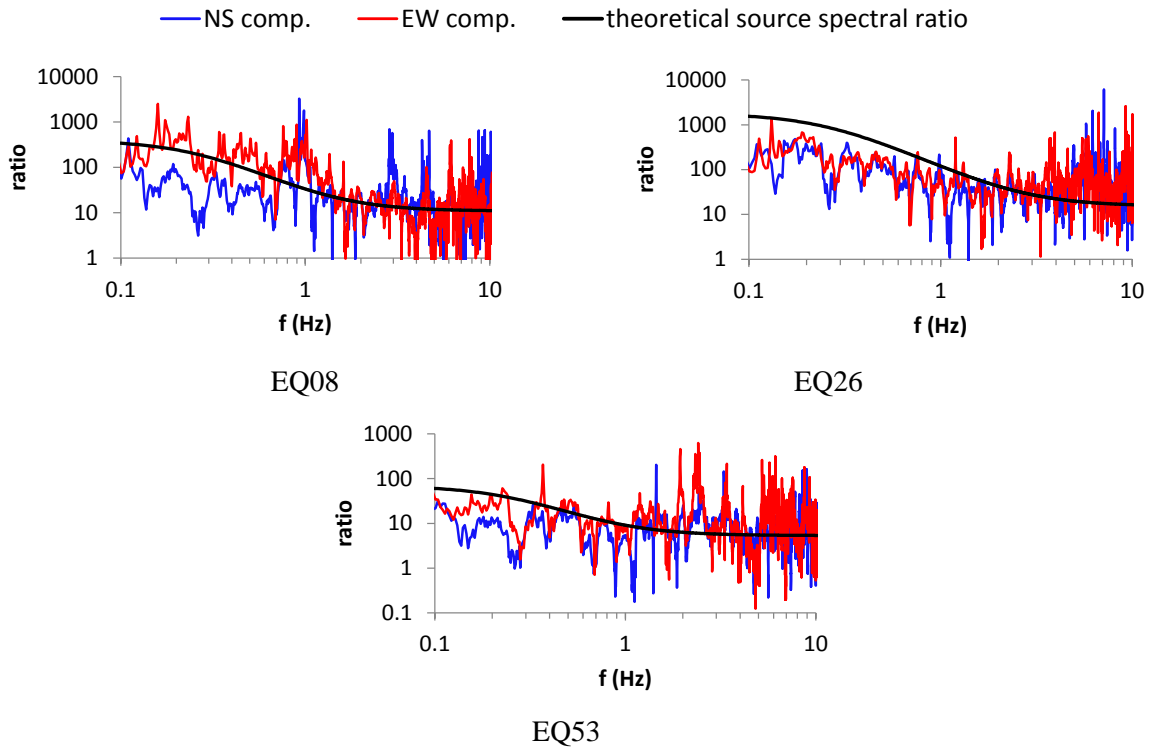


Figure 4 – Ratio of the source spectrum of the main-shock to that of the elemental earthquake

Table 3 – Estimated source parameters of the elemental earthquakes

Parameters	EQ08	EQ26	EQ53	Basis
Seismic moment M_0 (Nm)	1.21E+17	2.64E+16	6.86E+17	NIED(2011, 2013)
Corner frequency of the source spectrum f_c (Hz)	1.5	2.7	0.9	According to the observed acceleration source spectra.
Seismic fault area S (km ²)	3.11	0.96	8.64	$S=M_0/\mu D$
Averaged slip D (m)	0.81	0.57	1.65	$D=4 \times A / (7\pi^2 \mu \beta^2)$
Averaged stress drop $\Delta\sigma$ (MPa)	53.7	68.4	65.8	$\Delta\sigma=7\pi/16 \times \mu D \times (\pi/S)^{0.5}$
Short-period spectral level A (Nm/s ²)	1.07E+19	7.60E+18	2.19E+19	$A=4\pi^2 \times M_0 \times f_c^2$

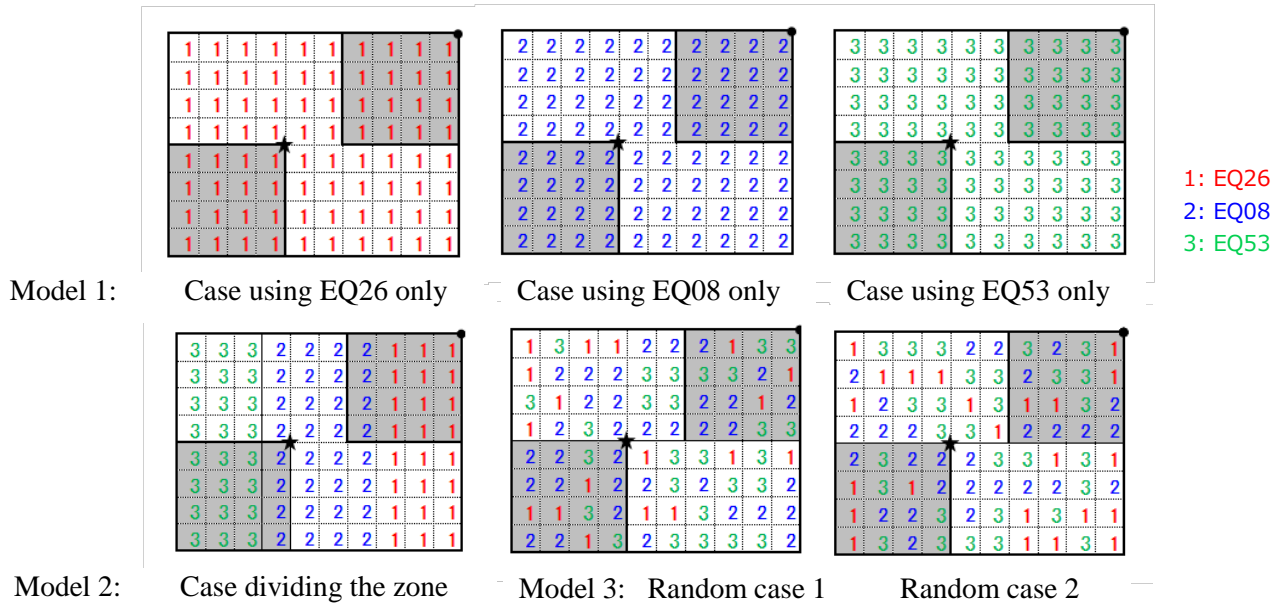


Figure 5 – Arrangements of the elemental earthquakes for the elemental faults in the fault model

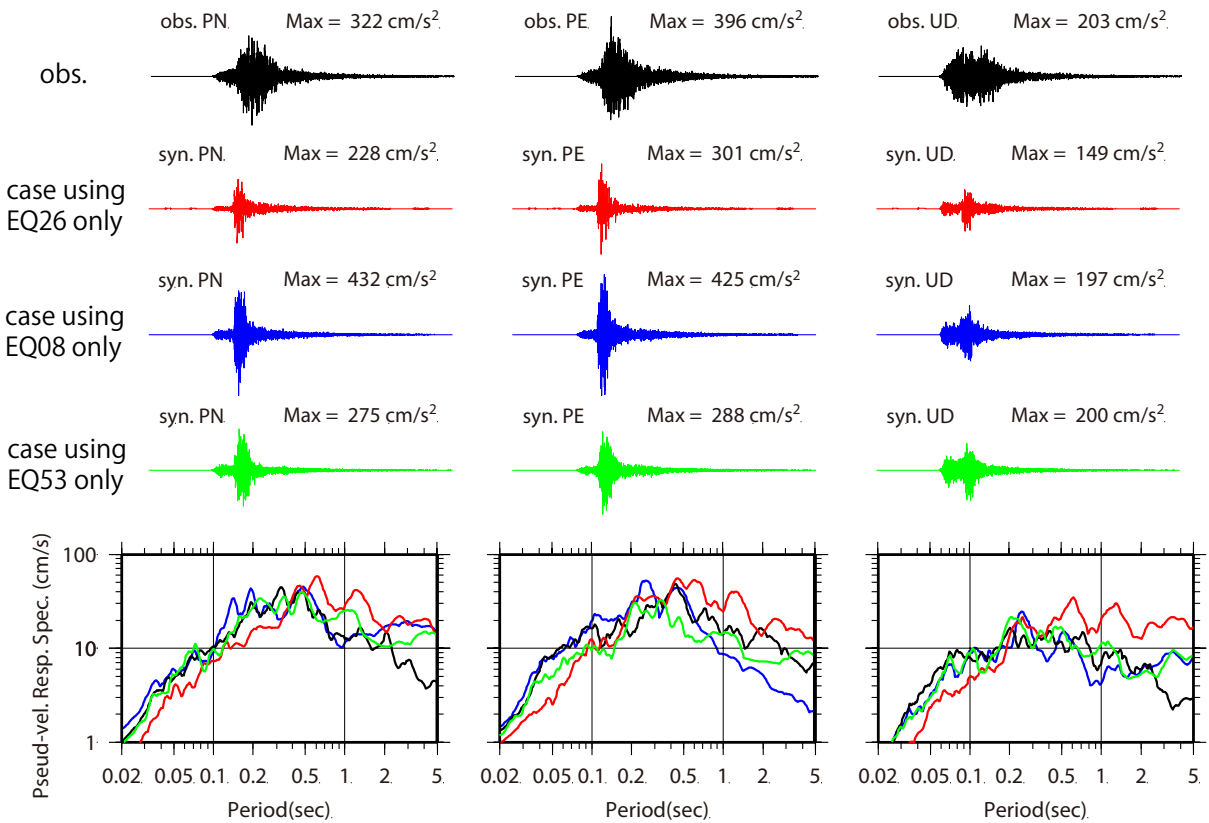


Figure 6 – Simulated strong motions of the model 1

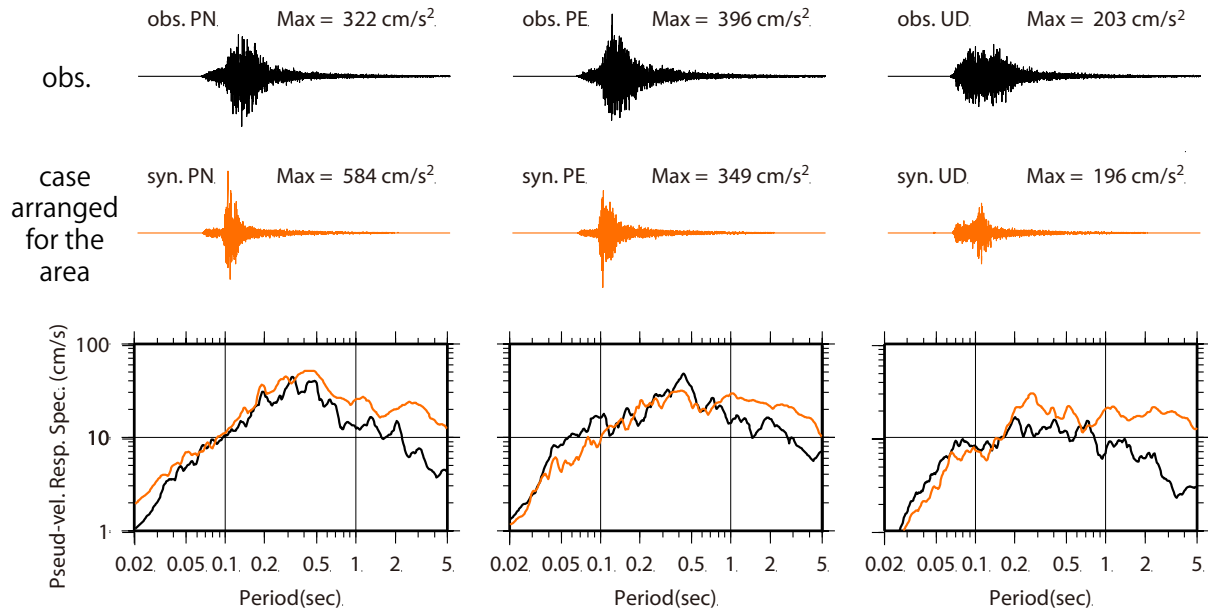


Figure 7 – Simulated strong motions of the models 2

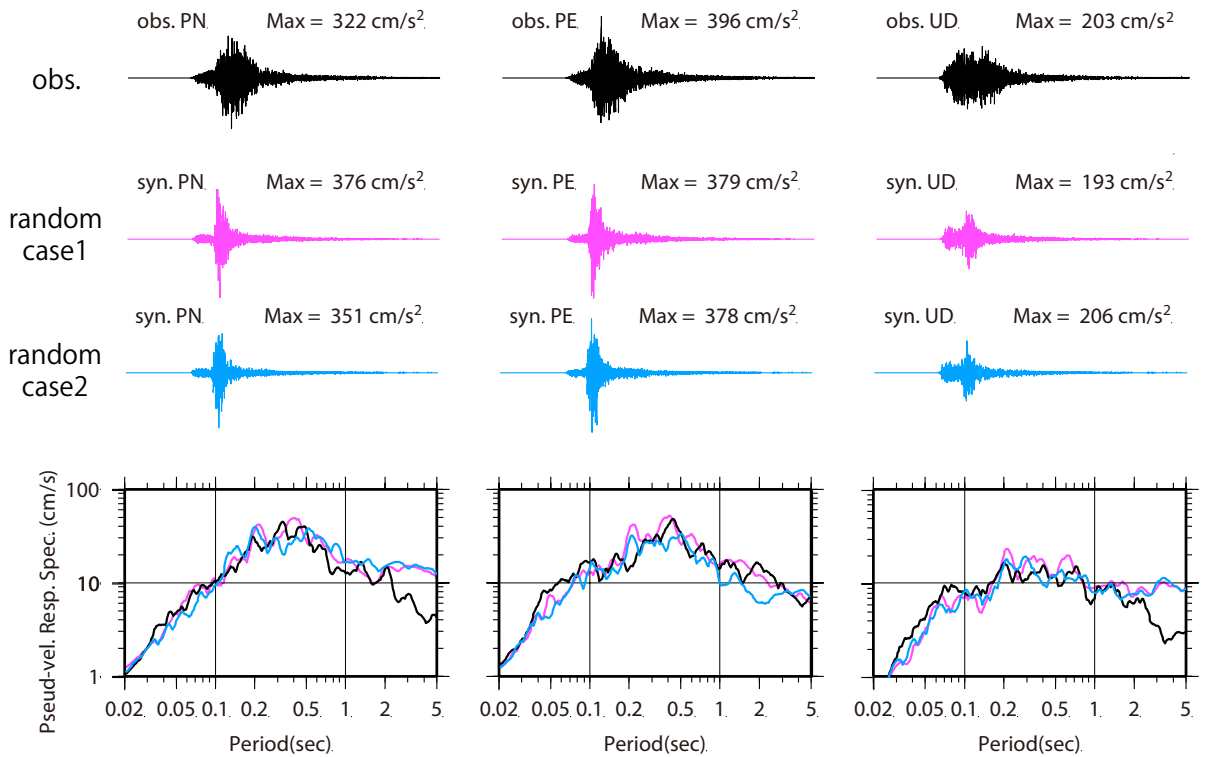


Figure 8 – Simulated strong motions of the models 3